Effect of Hot Rolling on the Microstructure and Mechanical Properties of a Ti-15Mo/TiB Metal-Matrix Composite

Sergey Zherebtsov [1] , **Maxim Ozerov** [1,*], **Elizaveta Povolyaeva** [1], **Vitaly Sokolovsky** [1], **Nikita Stepanov** [1] , **Dmitry Moskovskikh** [2] **and Gennady Salishchev** [1]

[1] Laboratory of Bulk Nanostructured Materials, Belgorod State University, Belgorod 308015, Russia; zherebtsov@bsu.edu.ru (S.Z.); lizapovolyaeva@gmail.com (E.P.); sokolovskiy@bsu.edu.ru (V.S.); stepanov@bsu.edu.ru (N.S.); salishchev@bsu.edu.ru (G.S.)

[2] National University of Science and Technology, Centre of Functional Nanoceramics, Moscow 119049, Russia; mos@misis.ru

* Correspondence: ozerov@bsu.edu.ru; Tel.: +7-919-223-8528

Abstract: A Ti-15Mo/TiB metal matrix composite was produced by the spark plasma sintering process at 1400 °C using a Ti-14.25 wt.% Mo-5 wt.% TiB_2 powder mixture. The microstructure and mechanical properties of the composite were studied after non-isothermal rolling of specimens heated to 1000 °C to a thickness strain of ~0.7. Transmission and scanning electron microscopy, as well as X-ray analysis were used for microstructure examination; mechanical properties were evaluated using tensile testing and microhardness measurement. In the initial condition, the Ti-15Mo/TiB composite consisted of 8.5 vol.% of TiB needle-like particles heterogeneously distributed within the β matrix. A small volume of fractions of the α″ and ω phases was also found in the microstructure. Microstructure evolution of the composite during hot rolling was associated with dynamic recrystallization of the bcc titanium matrix and shortening of the TiB whiskers by a factor of ~2. The Ti-15Mo/TiB composite after hot rolling showed considerable improvement in ductility without substantial loss of strength and hardness. The hot rolled specimen was not fractured during the compression test even after 45% thickness reduction, while in the initial condition, the compression ductility was 22%. The yield strength for both conditions was quite similar (~1350 MPa). The hot rolled composite also showed some improvement in ductility to ~12% elongation at elevated temperature (500 °C) compared to the initial condition, the tensile elongation of which did not exceed 2%. The observed difference in the mechanical behavior was associated with the presence of the metastable α″ and isothermal ω phases in the initial condition and the more stable α phase in the hot rolled condition.

Keywords: titanium matrix composite; beta titanium; deformation; microstructure; mechanical properties

1. Introduction

Titanium and titanium alloys are widely used in various industries due to a combination of high specific strength and excellent corrosion resistance [1]. However, relatively low absolute values of strength and hardness can limit titanium alloy applications. One way to overcome this problem is to create Ti based composites reinforced by ceramic particles [2–4]. Due to an almost perfect match (in terms of properties and crystallography) with the titanium matrix, TiB reinforcements have an advantage over other options [4,5]. In addition, TiB whiskers can be produced during sintering via the in situ Ti + TiB_2 → 2TiB reaction [6,7]. A promising method of producing relatively abundant

specimens of Ti/TiB composites is plasma spark sintering (SPS). The combination of a high rate of heating/cooling with high pressure can result in sintering at relatively low temperatures during a short time interval, thereby preserving the fine structure of the initial powders [8,9].

Meanwhile, achieving considerably increased strength and hardness of Ti/TiB composites results in loss in ductility, even in the case of a relatively low amount of reinforcements [10]. Some increase in ductility of Ti/TiB composites can be attained via thermomechanical treatment [11–14]. For example, the ductile-to-brittle transition temperature of a Ti-17 vol.% TiB composite was noticeably decreased due to warm multiaxial forging (MAF) [13,14]. However, room temperature ductility of warm/hot worked composites with ~17 vol.% TiB reinforcements was found to be low [15]. More practical and feasible hot/warm rolling can also improve the mechanical properties of Ti/TiB composites. Both ductility and strength were increased in a Ti/TiB composite with 12 vol.% of reinforcements due to a rolled thickness reduction of 80% [15]. Hot rolling of a titanium matrix composite with 7.5 vol.% TiB (the matrix was a Ti-6Al-2.5Sn-4Zr-0.7Mo-0.3Si-0.2Y alloy) in the β phase field attained approximately 5% tensile ductility [16].

Another possible way to improve the ductility of Ti/TiB composites is to exchange a hard-to-deform hcp α-Ti matrix for a more ductile bcc β-Ti matrix. In the case of powder metallurgy (for example, the SPS process), the bcc matrix can be attained due to the addition of a certain amount of β stabilizing element in the powder mixture. However, there is no information in the literature on the microstructure and mechanism of deformation of Ti based composite with bcc matrix. The Ti-15Mo alloy seems to be a promising option for use as the matrix; this alloy, with attractive mechanical properties, was developed for biomedical applications [17,18]. Due to a rather high concentration of β stabilizing Mo, the matrix can contain, apart from the β phase, the metastable ω phase (athermal or isothermal), which can transform under aging at elevated temperatures into the stable α phase [19]. In addition, α'' or even α' martensitic phase formation can be expected in Mo leaned areas as a result of the microstructural heterogeneity sometimes observed in specimens obtained by SPS [20].

Therefore, the aim of the present work was to study the microstructure and mechanical properties of a Ti-15Mo/TiB composite after hot rolling and to establish whether thermomechanical treatment can improve the ductility of this composite without considerable loss of strength and hardness. The composite containing 8.5 vol.% TiB reinforcement was produced by the SPS process at 1400 °C.

2. Materials and Procedure

A mixture of Ti (99.1% purity), Mo (99.95% purity), and TiB_2 (99.9% purity) powders was used for the composite production. The fractions of elements were 80.75 wt.% Ti and 14.25 wt.% Mo (to produce a Ti-15 wt.% Mo matrix alloy) and 5 wt.% TiB_2 (which gave 8.5 vol.% TiB) [21]. The mean size of the particles was 25 μm (Ti), 7 μm (TiB_2), and 3 μm (Mo) (Figure 1). The amount of reinforcement was chosen based on data in the literature for α-Ti/TiB composites to obtain high strength/hardness and sufficient ductility [21]. The mixture was obtained using a Retsch RS200 vibrating cup mill (Retsch, Haan, Germany) in ethanol; the speed of milling rotation was 700 rpm, and the mixing duration was 1 h.
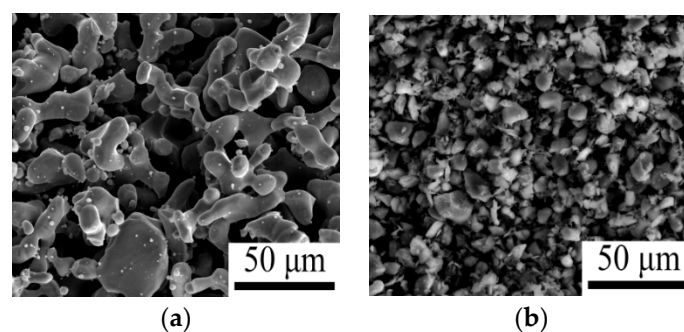

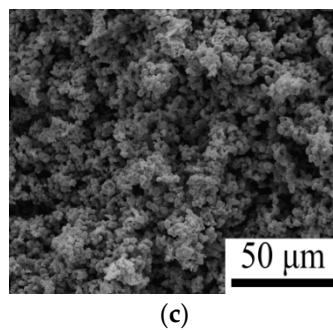(a)　　　　　　　　　　　　　　　　　　　　　　(b)

Figure 1. *Cont.*

(**c**)

Figure 1. SEM images of (**a**) Ti, (**b**) TiB$_2$, and (**c**) Mo powders.

The SPS process was carried out in a vacuum at 1400 °C for 15 min at 40 MPa using a Thermal Technology SPS 10-3 apparatus (Thermal Technology, LLC, Santa Rosa, CA, USA). The size of the obtained specimens was 39 mm in diameter and 25 mm in height (Figure 2a). The residual porosity, measured by hydrostatic weighing on a Porotech 3.1 Automated Standard Porosimeter and metallographic analysis, did not exceed 0.5%. Measured density was 4.756 g/cm^3. To improve the homogeneity of the specimens, they were annealed at 1200 °C for 24 h in argon. The homogenized state is referred to as the initial condition hereafter.

Prismatic samples measuring $4 \times 10 \times 30$ mm^3 were cut out from the homogenized cylinders using a Sodick AQ300L electro-discharge apparatus (Sodick Inc., Schaumburg, IL, USA). The samples were then heated to 1000 °C and rolled in non-isothermic conditions to a total thickness strain of 0.7 (55% thickness reduction). Unidirectional multipass rolling was performed using a reduction per pass of ~0.25 mm with 10 min holding in a furnace heated to 1000 °C after every 2 passes. Further rolling (above 55% thickness reduction) resulted in the formation of surface cracks on the side faces, most likely because of considerable cooling of the surface layers during non-isothermic deformation.

The microstructure under initial and deformed conditions was determined using transmission and scanning electron microscopy (TEM, SEM) and X-ray diffraction (XRD). TEM was done on a JEOL JEM 2100 microscope (JEOL, Tokyo, Japan); the specimens were obtained using twin jet electro-polishing in a mixture of 6% perchloric acid, 59% methanol, and 35% butanol at −35 °C and 29.5 V. SEM was carried out using an FEI Quanta 600 FEG microscope (Thermo Fisher Scientific, Hillsboro, OR, USA). The specimens for SEM were prepared by careful mechanical polishing; etching was performed using Kroll's reagent (95% H$_2$O, 3% HNO$_3$, 2% HF). XRD was carried out on an ARL-Xtra diffractometer (Thermo Fisher Scientific, Portland, OR, USA) with Cu-Kα radiation. The Rietveld method [22] was used for quantitative determination of the phase composition; the value of the experimental error was below ±2%.

The size of Ti grains and diameter and apparent length of TiB whiskers were calculated using SEM images. The linear intercept method (lengths along or across each particle) was used to determine the average grain size and length or thickness of the TiB whiskers. A total area of approximately 1000 μm^2 was examined for each condition.

Vickers microhardness was measured at room temperature using a 1000 g load for 10 s; 10 measurements were made for each specimen.

Dog bone shaped flat tensile specimens (Figure 2b) with a gauge measuring $4 \times 3 \times 1.5$ mm^3 were cut out of the rolled plates so that the rolling direction coincided with the tensile axis. Tensile tests were carried out using an Instron 5882 universal testing machine at 400 or 500 °C at a nominal strain rate of 10^{-3} s^{-1}. Compression tests of both conditions of the composite were conducted at room temperature and a nominal strain rate of 10^{-4} s^{-1} on the Instron 5882 machine using specimens measuring $1.5 \times 1.5 \times 3$ mm^3 (size was limited by the thickness of the hot rolled plate).

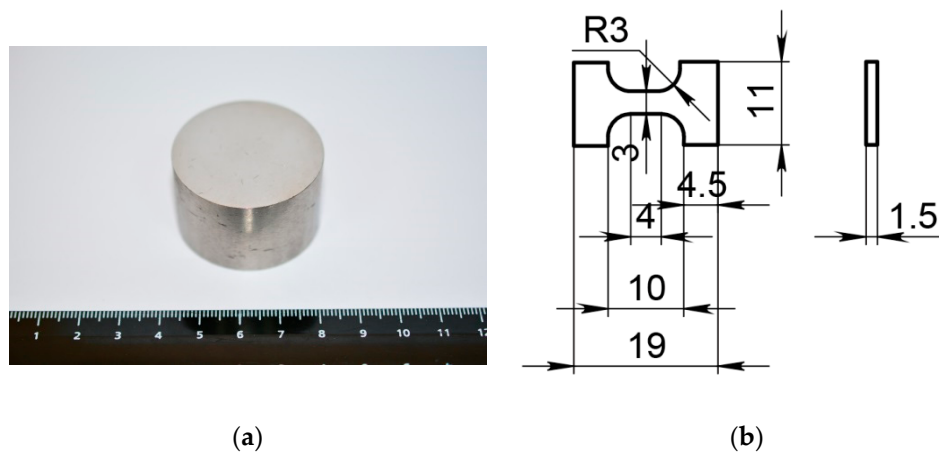(**a**)   (**b**)

Figure 2. (**a**) Sintered Ti-15Mo/TiB composite and (**b**) scheme of the tensile specimen (dimensions in mm).

3. Results

As per XRD data, the composite consisted mainly of the bcc Ti matrix with ~8.5 vol.% of TiB (Figure 3). The TiB reinforcement had a needle-like shape with an average thickness of 400 ± 200 nm (Figure 4a,b). Some TiB whiskers were rather thick (up to few micrometers), and arbitrary cross-sections of these whiskers could be seen as almost equiaxial coarse TiB particles. The apparent length of the TiB whiskers, heterogeneously distributed in the β-Ti matrix, was 5 ± 2 μm. The average grain size in the bcc Ti matrix was evaluated to be 14 ± 6 μm. At some grain boundaries, thin lamellar precipitations of the α″ phase were observed (Figure 4a). The volume fraction of the martensitic phase was evaluated to be lower than 2%; although this amount was not reliably detected by X-ray diffraction, some tiny peaks in the XRD pattern could be ascribed to the α″ phase. Some pores adjacent to TiB particles were also found (see the upper right corner of Figure 4a); their formation could be attributed to the Kirkendall effect [23].

TEM also showed the bcc Ti matrix, which contained randomly arranged TiB whiskers. Increased dislocation density was often observed near the TiB whiskers (Figure 4c). The average distance between adjacent TiB whiskers (which can be considered as a free dislocation path to a first approximation) was evaluated to be ~0.5–0.7 μm. The α″ precipitations with an average thickness of ~200 nm (Figure 4d) were observed at some borders of the former particles. In addition, very small equiaxed ω phase particles measuring ~10 nm in diameter were found in the microstructure (Figure 4e). However, it should be noted that the distribution of these particles was rather heterogeneous; besides, the presence of the ω phase was not reliably detected by XRD (possible positions are shown by arrows in Figure 3), due to both a low fraction and overlapping with some β peaks (Figure 3).
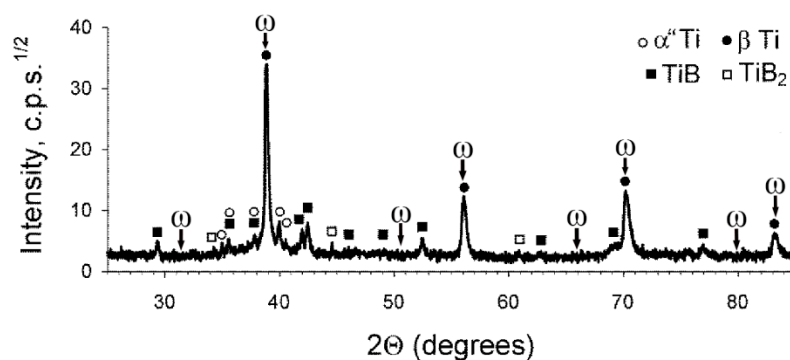

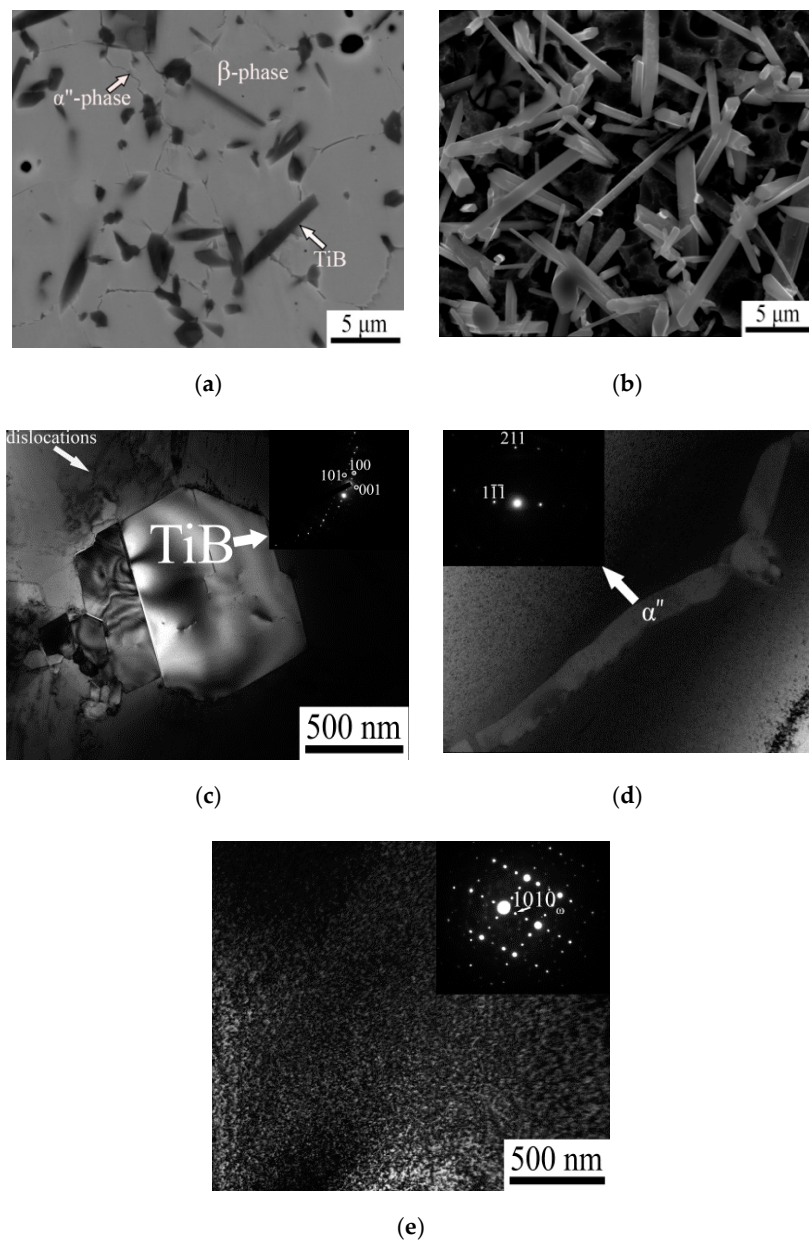**Figure 3.** XRD patterns of Ti-15Mo/TiB metal matrix composite.

Figure 4. Microstructure of Ti-15Mo/TiB composite in initial condition: (**a**) SEM image of unetched surface; (**b**) SEM image of the etched surface; (**c–e**) TEM field images and selected area diffraction pattern of the TiB, α″, and ω phases, respectively.

Hot rolling resulted in some elongation of the matrix grains toward the metal flow direction and a decrease in the bcc grain size to 12 ± 6 μm (Figure 5a). Elongated TiB particles also became aligned with the rolling direction; coarse particles mostly decorated bcc grain boundaries. Cracks formed in TiB particles (Figure 5b) could possibly initiate secondary cracks in the β matrix (shown in Figure 5b by a black arrow). Some round pores around TiB particles most likely were inherited from the initial condition. The apparent length of the TiB particles decreased to 3.0 ± 1.2 μm due to the formation of transverse cracks and breaking of the whiskers (Figure 5a,c). Hot deformation also resulted in the appearance of ~7% of the α phase in the β matrix (Figure 5d), while any signs of the α″ and ω phases were not observed in the XRD pattern.
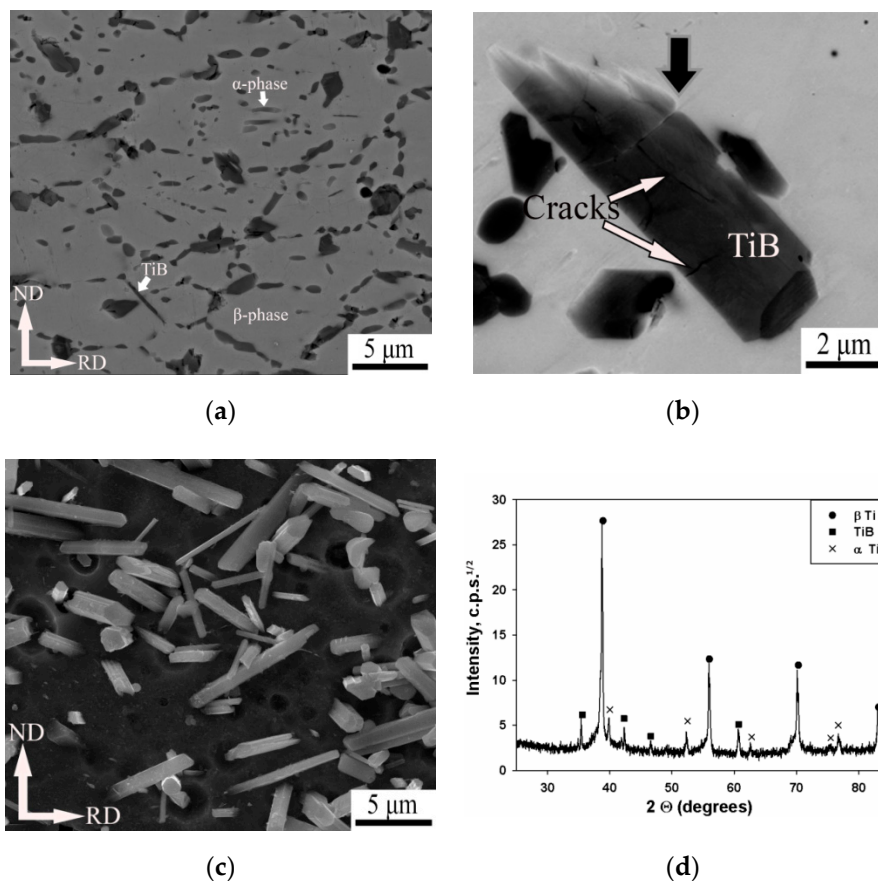
Figure 5. (**a**–**c**) SEM microstructure and (**d**) XRD pattern of Ti-15Mo/TiB metal matrix composite after hot rolling: (**a**,**b**) unetched surface; (**c**) etched surface. Rolling direction for all images is shown in the bottom-left corner of (**c**).

TEM showed the development of dynamic recrystallization in the bcc Ti matrix during hot rolling with the formation of a coarse grained structure with very low dislocation density (Figure 6a). No pores or cracks were observed along interphase Ti/TiB boundaries. The α phase in the form of rather thin (~300 nm) lamellae was distributed in the microstructure quite heterogeneously (Figure 6b).
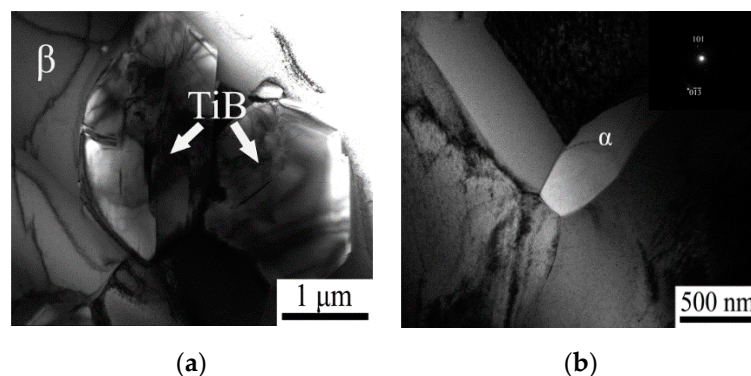

Figure 6. TEM images of Ti-15Mo/TiB composite microstructure after hot rolling.

The microhardness of Ti-15Mo/TiB metal matrix composite increased by ~36% in comparison with Ti-15Mo obtained by SPS (Table 1; it should be noted, however, that the hardness of cast Ti-15Mo was even lower, ~310 HV [24]). The microhardness of Ti-15Mo/TiB composite was also higher by ~17% compared to hcp α-Ti/TiB composite with the same amount of TiB. However, microhardness was found

to be decreased by ~10% as a result of hot rolling, most probably due to factors that resulted in increased ductility (i.e., recrystallization of the β matrix and shortening/redistribution of the TiB particles).

Table 1. Microhardness characteristics of samples with various compositions.

Condition	Microhardness (HV)
Ti-15Mo	353 ± 8
Ti/8.5 vol.% TiB	413 ± 10
Ti-15Mo/8.5 vol.% TiB	481 ± 10
Ti-15Mo/8.5 vol.% TiB + Hot rolling	429 ± 9

Stress–strain curves of the Ti-15Mo/TiB composite in the initial and hot rolled conditions obtained during uniaxial compression at room temperature are shown in Figure 7a. For comparison, a typical stress–strain curve for an hcp α Ti/TiB composite with the same volume fraction of TiB reinforcement is also presented (details of the experiment can be found elsewhere [13,14]). One can see that after hot rolling, the composite showed some increased flow stress and considerably improved ductility. The specimen was not fractured even after 45% thickness reduction, while compression ductility for the initial condition was 22%. The yield strength for both conditions was quite similar however (1330 MPa for hot rolled and 1360 MPa for initial condition). Some instability of plastic flow after ~20% of height reduction (most probably associated with localized shear deformation) on the curve corresponding to the hot rolled specimen should be noted; however, no surface cracks were observed after compression testing. Compared to the hcp α titanium based composite, both conditions of the bcc β titanium based composite showed much higher strength and ductility; the yield strength of the α-Ti/TiB was 970 MPa, and the height reduction was 9% (Figure 7a).
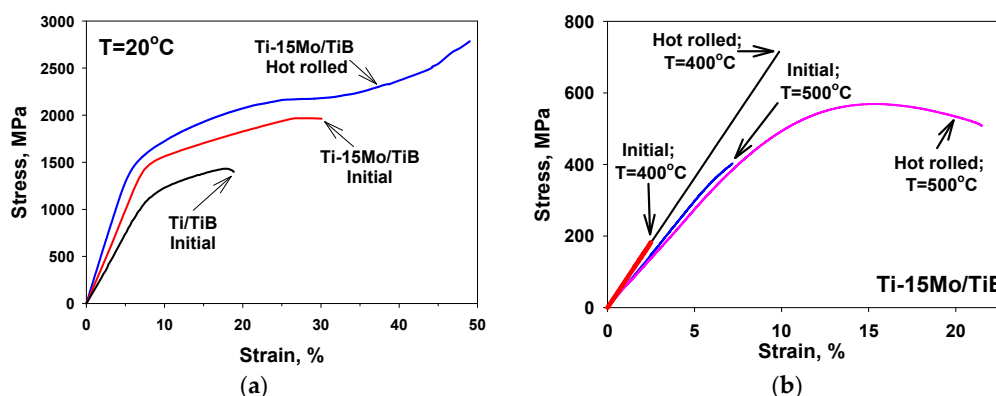

Figure 7. Stress–strain curves of Ti-15Mo/TiB composite in initial and hot rolled conditions tested (**a**) in compression at room temperature and (**b**) in tension at 400 or 500 °C. A typical stress–strain curve for hcp α Ti/TiB composite with the same volume fraction of TiB reinforcement is shown in (**a**) for comparison.

High temperature mechanical properties of the composite were also noticeably changed as a result of hot rolling (Figure 7b). Although at 400 °C, neither condition of the alloy showed a plastic flow stage, specimens after hot rolling fractured at much higher stresses than in the initial condition. Increased deformation temperature of 500 °C resulted in very limited ductility (less than 1% elongation) in the initial condition. Meanwhile, a hot rolled specimen showed pronounced tensile elongation of ~12%. At the same time, quite fast plastic flow localization observed in the composite suggested limited hardening capacity of the material. The value of ultimate tensile strength of the composite at 500 °C was found to be ~570 MPa.

Analysis of the fracture surface showed considerably different fracture characteristics in the initial and hot rolled conditions (Figure 8). The fracture surface of the initial condition was typical of brittle fracture, with cleavage facets and some obvious river patterns (Figure 8a). In some places, the observed

relief could be ascribed to intercrystalline fracture. After hot rolling, the fracture became more ductile, with the formation of characteristic dimples (Figure 8b). It should be noted that cracks along Ti/TiB interfaces were not observed in either condition; however, cracks in the Ti particles could propagate into the β matrix during deformation (see Figure 5b). Besides, the strain incompatibility between the soft and ductile bcc β titanium matrix and hard TiB most likely resulted in strain localization and further fracture of the matrix near the interfaces; grooves around some TiB particles could be formed as a result of this process (shown by black arrows in Figure 8a,b).
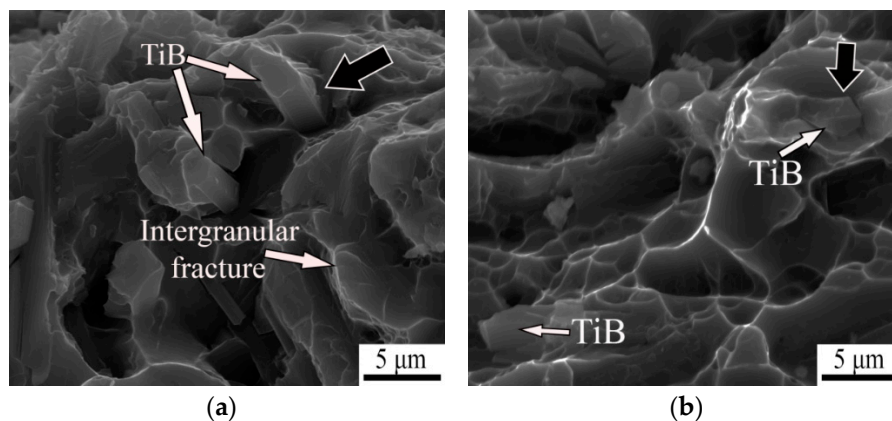

(**a**)　　　　　　　　　　　　　　　　(**b**)

Figure 8. Fracture surfaces of tensile tested specimens at 500 °C (**a**) in as-sintered condition and (**b**) after hot rolling. Grooves around TiB particles are shown with black arrows.

4. Discussion

The obtained results showed the improved mechanical properties of the Ti-15Mo/TiB composite subjected to non-isothermal rolling at an initial temperature of 1000 °C. The strength and hardness of the composite did not change noticeably due to rolling (Figure 7, Table 1), most probably because of the relatively high processing temperature, which prevented considerable refinement of the bcc grains and shortening of the TiB whiskers (compare Figures 4a and 5a). However, the hot worked composite showed both considerable compressive ductility (more than 45% of height reduction) at room temperature and substantial tensile elongation at 500 °C (~12%). Meanwhile, the height reduction at room temperature and tensile elongation of as-sintered and homogenized Ti-15Mo/TiB at 500 °C did not exceed 22 and 2%, respectively (Figure 7). More ductile behavior of the hot rolled composite was also confirmed by the formation of a ductile fracture surface (Figure 8b) after tension at 500 °C in contrast to cleavage facets in the initial condition (Figure 8a).

Some improvement in the mechanical properties of Ti based metal matrix composites reinforced by TiB particles due to thermomechanical treatments has been reported several times [11–16]. For example, some (~3%) ductility was observed during compression at room temperature of a Ti based composite with 17 vol.% of TiB after hot MAF; in the spark plasma sintering condition, this composite was fractured in the elastic region [14]. A moderate decrease (by ~100 °C) in the brittle-ductile transition as a result of thermomechanical treatment of the composite was also reported in [13]. In these cases, the improved ductility was ascribed to recrystallization of the Ti matrix and shortening/redistribution of the TiB whiskers [14]. Although all these studies focused on composites with hcp α-Ti matrix, the same factors (recrystallization of the matrix and shortening of the TiB whiskers) could obviously have contributed to the improved ductility of the Ti-15Mo/TiB composite in our case.

Meanwhile, the addition of the second refractory element to the titanium matrix could change the mechanism of deformation and strengthening factors operating in the composite considerably. Basically, the addition of 15 wt.% Mo to the Ti matrix resulted in hcp-to-bcc transition [25], which ensured better deformability due to a greater number of slip systems. Some increase in the ductility of Ti-Mo alloys could also be expected due to the activation of deformation twinning ({332} <113> system) [26]. On the other hand, solid solution hardening should increase the strength of a composite

with the Ti-15Mo matrix. Another powerful factor contributing to strength was ω phase formation; however, this could also result in composite embrittlement, which is not desirable [27].

The SPS process did not necessarily result in the formation of a completely homogeneous microstructure. Refractory elements required higher temperatures and a much longer time (compared to SPS) to distribute uniformly. High temperature annealing obviously improved the distribution of chemical elements in the composites; however, some variations still existed. Most likely, this heterogeneity in the initial condition resulted in the formation of such metastable phases as α″ and isothermal ω (Figure 4d,e) during cooling from the annealing temperature (1200 °C) [28]. The presence of the relatively soft α″ martensitic phase (compared to the harder α′ [25]) along some grains could result in intergranular fracture, while the ω phase was responsible for the formation of cleavage facets (Figure 8a). Non-isothermal hot working made the Mo distribution more homogeneous, resulting in the formation of α lamellae in the β matrix. This condition of the alloy showed both higher compression ductility at room temperature and tensile elongation at temperatures ≥ 500 °C, typical of annealed two phase titanium alloy ductile fracture (Figure 8b) [29].

Room temperature mechanical properties of different Ti based metal matrix composites with different volume fractions of TiB (in terms of yield strength vs. ductility) are collected in Figure 9. Both elongation to fracture (in the case of tensile tests) and height reduction (in the case of compression tests) were used to evaluate ductility. The compressive strength and ductility were expectedly higher than those determined in tension. An increase in TiB content resulted in higher strength and lower ductility. However, one can clearly see that using the bcc β-Ti matrix resulted in a very good combination of ductility and strength even in the initial (homogenized) condition, which became much better due to hot rolling. The volume fraction of TiB in this composite was quite low (8.5 vol.%) and could probably be increased to improve the strength without compromising ductility [21,30]. However, further studies are needed to establish the optimal phase composition in the composite for the best strength-ductility balance.
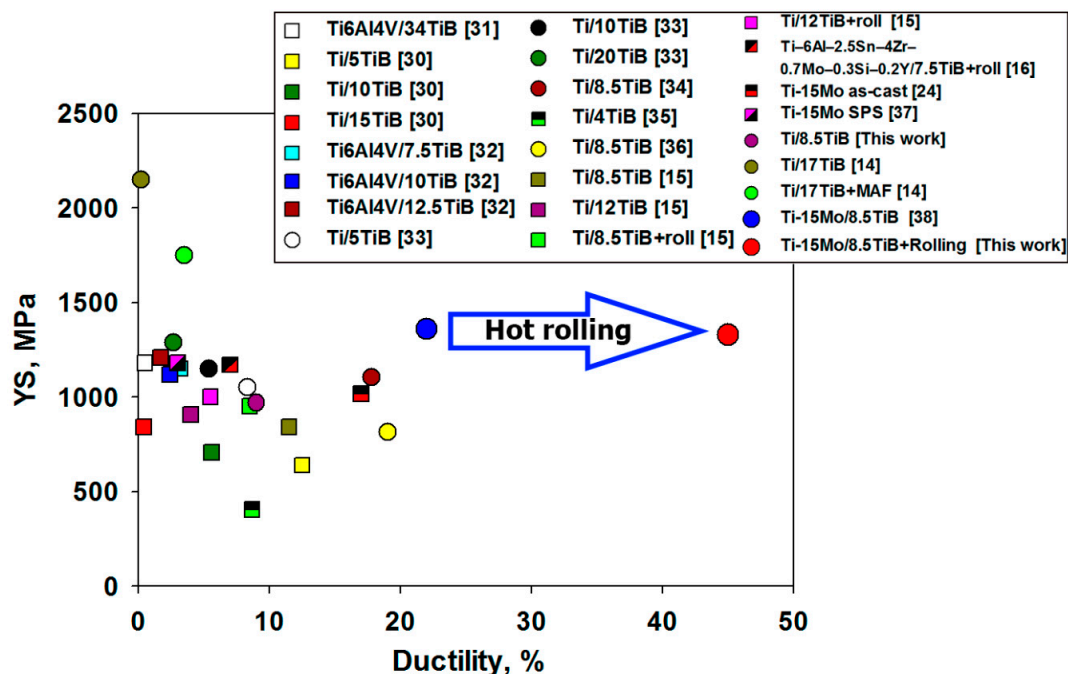

Figure 9. Room temperature mechanical properties of Ti based metal matrix composites reinforced with TiB in terms of yield strength (YS) vs. ductility. Elongation to fracture in the case of tensile tests (squares) and height reduction in the case of compression tests (circles) were used to determine ductility [14–16,30–38]. The composition of the matrix (hcp α-Ti, Ti-6Al-4V, and Ti-15Mo) and volume fractions of the TiB are shown in the legend.

5. Conclusions

(1) The initial microstructure of the Ti-15Mo/TiB composite consisted of ~8.5 vol.% of TiB needle-like particles heterogeneously distributed within the β matrix. The average diameter and mean apparent length of the TiB whiskers were 400 ± 200 nm and 5 ± 2 μm, respectively. The average grain size in the bcc Ti matrix was evaluated to be 14 ± 6 μm. In addition, small volume fractions of the α″ and ω phases were found in the microstructure.

(2) Microstructure evolution of the composite during hot rolling was associated with dynamic recrystallization of the bcc titanium matrix, due to which the average grain size decreased to 12 ± 6 μm and TiB whiskers shortened to 3 ± 1.2 μm. Hot deformation also resulted in the formation of ~7% of the α phase in the β matrix.

(3) Non-isothermal rolling of Ti-15Mo/TiB composite at a starting temperature of 1000 °C to a cumulative strain of ~0.7 resulted in considerably increased strength and ductility during the compression test at room temperature and tensile ductility without substantial loss in strength during tension at 500 °C. For instance, the hot rolled specimen was not fractured even after 45% thickness reduction, while the initial condition was 22%. The yield strength was 1330 MPa for the hot rolled and 1360 MPa for the initial condition. At 500 °C, tensile elongation of only 2% was obtained in the as-sintered specimen, whereas the specimen after hot rolling demonstrated tensile elongation of 12.5% at the same temperature.

References

1. Leyens, C.; Peters, M. *Titanium and Titanium Alloys: Fundamentals and Applications*; Wiley-VCH: Weinheim, Germany, 2003; pp. 1–499.

2. Morsi, K.; Patel, V.V. Processing and properties of titanium-titanium boride (TiBw) matrix composites—A review. *J. Mater. Sci.* **2007**, *42*, 2037–2047. [CrossRef]

3. Saito, T.; Furuta, T.; Yamaguchi, T. Development of low cost titanium matrix composite. In *Advances in Titanium Metal Matrix Composites, the Minerals, Metals and Materials Society*; Froes, F.H., Storer, J., Eds.; TMS: Warrendale, PA, USA, 1995; pp. 33–44.

4. Godfrey, T.M.T.; Goodwin, P.S.; Ward-Close, C.M. Titanium Particulate Metal Matrix Composites—Reinforcement, Production Methods, and Mechanical Properties. *Adv. Eng. Mat.* **2000**, *2*, 85–91. [CrossRef]

5. Morsi, K. Review: Titanium–titanium boride composites. *J. Mater. Sci.* **2019**, *54*, 6753–6771. [CrossRef]

6. Feng, H.; Zhou, Y.; Jia, D.; Meng, Q.; Rao, J. Growth mechanism of in situ TiB whiskers in spark plasma sintered TiB/Ti metal matrix composites. *Cryst. Growth Des.* **2006**, *6*, 1626–1630. [CrossRef]

7. Radhakrishna Bhat, B.V.; Subramanyam, J.; Bhanu Prasad, V.V. Preparation of Ti-TiB-TiC & Ti-TiB composites by in-situ reaction hot pressing. *Mater. Sci. Eng. A* **2002**, *325*, 126–130. [CrossRef]

8. Ravi Chandran, K.S.; Panda, K.B.; Sahay, S.S. TiBw-reinforced Ti composites: Processing, properties, application, prospects, and research needs. *JOM* **2004**, *56*, 42–48. [CrossRef]

9. Yang, Y.F.; Qian, M. Spark plasma sintering and hot pressing of titanium and titanium alloys. *Titan. Powder Metall.* **2015**, 219–235. [CrossRef]

10. Ozerov, M.; Stepanov, N.; Kolesnikov, A.; Sokolovsky, V.; Zherebtsov, S. Brittle-to-ductile transition in a Ti–TiB metal matrix composite. *Mater. Lett.* **2017**, *187*, 28–31. [CrossRef]

11. Gaisin, R.A.; Imayev, V.M.; Imayev, R.M. Effect of hot forging on microstructure and mechanical properties of near α titanium alloy/TiB composites produced by casting. *J. Alloys Compd.* **2017**, *723*, 385–394. [CrossRef]

12. Zherebtsov, S.; Ozerov, M.; Stepanov, N.; Klimova, M.; Ivanisenko, Y. Effect of high-pressure torsion on structure and microhardness of Ti/TiB metal matrix composite. *Metals* **2017**, *7*, 507. [CrossRef]

13. Zherebtsov, S.; Ozerov, M.; Stepanov, N.; Klimova, M. Structure and properties of Ti/TiB metal–matrix composite after isothermal multiaxial forging. *Acta Phys. Pol. A* **2018**, *134*, 695–698. [CrossRef]

14. Ozerov, M.; Klimova, M.; Sokolovsky, V.; Stepanov, N.; Popov, A.; Boldin, M.; Zherebtsov, S. Evolution of microstructure and mechanical properties of Ti/TiB metal matrix composite during isothermal multiaxial forging. *J. Alloys Compd.* **2019**, *770*, 840–848. [CrossRef]

15. Huang, L.; Cui, X.; Geng, L.; Fu, Y. Effects of rolling deformation on microstructure and mechanical properties of network structured TiBw/Ti composites. *Trans. Nonferrous Met. Soc. China* **2012**, *22*, 79–83. [CrossRef]

16. Zhang, C.J.; Kong, F.T.; Xu, L.J.; Zhao, E.T.; Xiao, S.L.; Chen, Y.Y.; Deng, N.J.; Ge, W.; Xu, G.J. Temperature dependence of tensile properties and fracture behavior of as rolled TiB/Ti composite sheet. *Mater. Sci. Eng. A* **2012**, *556*, 962–969. [CrossRef]

17. Khorasani, A.M.; Goldberg, M.; Doeven, E.H.; Littlefair, G. Titanium in biomedical applications—properties and fabrication: A review. *J. Biomater. Tissue Eng.* **2015**, *5*, 593–619. [CrossRef]

18. Chen, Q.; Thouas, G.A. Metallic implant biomaterials. *Mater. Sci. Eng. R Rep.* **2015**, *87*, 1–57. [CrossRef]

19. Banerjee, S.; Mukhopadhyay, P. *Phase Transformations: Examples from Titanium and Zirconium Alloys*; Elsevier: Amsterdam, The Netherlands, 2007.

20. Zherebtsov, S.; Ozerov, M.; Klimova, M.; Stepanov, N.; Vershinina, T.; Ivanisenko, Y.; Salishchev, G. Effect of High-Pressure Torsion on Structure and Properties of Ti-15Mo/TiB Metal-Matrix Composite. *Materials* **2018**, *11*, 2426. [CrossRef]

21. Huang, L.J.; Geng, L.; Wang, B.; Wu, L.Z. Effects of volume fraction on the microstructure and tensile properties of in situ TiBw/Ti6Al4V composites with novel network microstructure. *Mater. Des.* **2013**, *45*, 532–538. [CrossRef]

22. Will, G. *Powder Diffraction: The Rietveld Method and the Two-Stage Method to Determine and Refine Crystal Structures from Powder Diffraction Data*; Springer: Berlin, Germany, 2005.

23. Ivasishin, O.M.; Markovsky, P.E.; Savvakin, D.G.; Stasiuk, O.O.; Rad, M.N.; Prikhodko, S.V. Multi-layered structures of Ti-6Al-4V alloy and TiC and TiB composites on its base fabricated using blended elemental powder metallurgy. *J. Mater. Process. Technol.* **2019**, *269*, 172–181. [CrossRef]

24. Gatina, S.A.; Semenova, I.P.; Joern, L.; Valiev, R.Z. Nanostructuring and Phase Transformations in the β-alloy Ti-15Mo during High-Pressure Torsion. *Adv. Eng. Mater.* **2015**, *17*, 1742–1747. [CrossRef]

25. Meyers, M.A.; Chawla, K.K. *Mechanical Behavior of Materials*; Cambridge University Press: New York, NY, USA, 2009.

26. Min, X.; Chen, X.; Emura, S.; Tsuchiya, K. Mechanism of twinning-induced plasticity in β-type Ti–15Mo alloy. *Scripta Mater.* **2013**, *69*, 393–396. [CrossRef]

27. Zwicker, U. *Titanium and Titanium Alloys*; Springer: Berlin, Germany, 1974.

28. Hickman, B.S. The Formation of Omega Phase in Titanium and Zirconium Alloys: A Review. *J. Mater. Sci.* **1969**, *4*, 554–563. [CrossRef]

29. Joshi, V.A. *Titanium Alloys: An Atlas of Structures and Fracture Feature*; Taylor & Francis Group: Boca Raton, FL, USA, 2006.

30. Kurita, H.; Suzuki, S.; Kikuchi, S.; Yodoshi, N.; Gourdet, S.; Narita, F. Strengthening mechanism of titanium boride whisker-Rreinforced Ti-6Al-4V alloy matrix composites with the TiB orientation perpendicular to the loading direction. *Materials* **2019**, *12*, 2401. [CrossRef] [PubMed]

31. Gorsse, S.; Miracle, D.B. Mechanical properties of Ti–6Al–4V/TiB composites with randomly oriented and aligned TiB reinforcements. *Acta Mater.* **2003**, *51*, 2427–2442. [CrossRef]

32. Tsang, H.T.; Chao, C.G.; Ma, C.Y. Effects of volume fraction of reinforcement on tensile and creep properties of in-situ TiB/Ti MMC. *Scr. Mater.* **1997**, *37*, 1359–1365. [CrossRef]

33. Jeong, H.W.; Kim, S.J.; Hyun, Y.T.; Lee, Y.T. Densification and compressive strength of in-situ processed Ti/TiB composites by powder metallurgy. *Met. Mater. Int.* **2002**, *8*, 25–35. [CrossRef]

34. Attar, H.; Bönisch, M.; Calin, M.; Zhang, L.-C.; Scudino, S.; Eckert, J. Selective laser melting of in situ titanium titanium boride composites: Processing, microstructure and mechanical properties. *Acta Mater.* **2014**, *76*, 13–22. [CrossRef]

35. Namini, A.S.; Azadbeh, M. Microstructural characterisation and mechanical properties of spark plasma-sintered TiB2-reinforced titanium matrix composite. *Powder Metall.* **2017**, *60*, 22–32. [CrossRef]

36. Attar, H.; Bönisch, M.; Calin, M.; Zhang, L.C.; Zhuravleva, K.; Funk, A.; Scudino, S.; Yang, C.; Eckert, J. Comparative study of microstructures and mechanical properties of in situ Ti–TiB composites produced by selective laser melting, powder metallurgy, and casting technologies. *J. Mater. Res.* **2014**, *29*, 1941–1950. [CrossRef]

37. Veverková, A.; Kozlík, J.; Bartha, K.; Chráska, T.; Corrêa, C.A.; Stráský, J. Mechanical properties of Ti-15Mo alloy prepared by cryogenic milling and spark plasma sintering. *Metals* **2019**, *9*, 1280. [CrossRef]

38. Zherebtsov, S.; Ozerov, M.; Klimova, M.; Moskovskikh, D.; Stepanov, N.; Salishchev, G. Mechanical behavior and microstructure evolution of a Ti-15Mo/TiB titanium matrix composite during hot deformation. *Metals* **2019**, *9*, 1175. [CrossRef]